Optimal Imaging Receiver Design for High-Speed Mobile Optical Wireless Communications

Mohammad Dehghani Soltani*, Hossein Kazemi†, Elham Sarbazi†, Harald Haas†, and Majid Safari*
*Institute for Digital Communications, School of Engineering, The University of Edinburgh, Edinburgh, UK
†LiFi R & D Centre, Department of Electronic & Electrical Engineering, University of Strathclyde, Glasgow, UK
*{m.dehghani, majid.safari}@ed.ac.uk,
†{h.kazemi, e.sarbazi, harald.haas}@strath.ac.uk.

***Abstract*—The optical receivers suitable for the next generation of optical wireless networks need to be ultra-high-speed while having a wide field of view (FOV) to accommodate user mobility. The design of such receivers is challenging due to two known trade-offs, namely, the area-bandwidth and the gain-FOV. In this study, we consider these trade-offs and formulate an optimisation problem to design imaging receivers that can achieve maximum high speed while satisfying a minimum FOV requirement. The design will be based on an array of arrays of photodetectors for which we present analytical derivations of signal-to-noise ratio (SNR) assuming maximum ratio combining (MRC). Practical considerations and non-idealities have been considered in our design and the reliability of the analytical model is verified by Optic Studio-based simulations. The optimization problem is solved assuming on-off keying (OOK) modulation. The results show a trade-off between achievable data rate and FOV. For example, it is demonstrated that a data rate of ~ 23 Gbps is achievable with a receiver of at most 2 cm $\times$ 2 cm dimensions with a FOV of 15°. However, a receiver with the same dimensions may only achieve ~ 8 Gbps if the FOV requirement increases to 20°.**

***Index Terms*—High-speed optical imaging receiver, wide field-of-view (FOV), array of photodetectors, optical wireless communications (OWCs).**

I. Introduction

The rapid increase in global demand for high-speed data rate has no saturation trends [1]. It is forecasted there will be 5.7 billion mobile devices by 2023 [2]. This results in a tremendous growth in data traffic of wireless communications. The radio frequency (RF) may struggle to cope with this high data traffic. RF spectrum is becoming more congested and wireless appliances are interfering with each other.

Optical wireless communication (OWC), which enables the use of a huge spectrum, is a promising solution to ease the RF spectrum congestion. Moreover, the coexistence of OWC and RF networks allows for the path to immense capacity growth, particularly for indoor scenarios to be unlocked [3]. OWC cooperates to offload heavy traffic from the congested RF wireless networks, as a consequence, making the room available for low-capacity streams such as the Internet of Things (IoT) [4].

High-speed aggregate Terabit per second indoor OWC networks are being realized by means of large modulation bandwidth laser diodes [5]–[8]. Hong *et al.* have demonstrated that a ten-channel wavelength division multiplexing (WDM) intensity modulation/direct detection (IM/DD) system achieves > 1 Tb/s capacity at a perpendicular distance of 3.5 m with a horizontal coverage up to 1.8 m [5]. A 1 Tbit/s bi-directional free-space connection is reported in [6], where ten WDM channels with pulse amplitude modulation (PAM)-4 are implemented. The coverage area of 2.54 m^2 is shown. Beam-steering laser-based optical systems, which are capable of supporting multiuser scenarios with 128 beams carrying up to 112 Gbit/s per beam is presented in [7]. These mentioned studies accentuate the potential of OWC as a key enabler to realize high-speed indoor networks for future sixth generation (6G) wireless systems. However, one of the major challenges in accomplishment of high-speed indoor OWC is to develop a portable receiver for mobile users.

Design of a high-speed and compact receiver to guarantee a required field of view (FOV) is fairly challenging due to two major reasons. Firstly, there is the well-known trade-off between photodetector (PD) bandwidth and its sensitive area. The second trade-off is between the optics gain and the FOV in accordance with the etendue law of conservation [9]. In other words, light-focusing optics (lens or concentartor) can compensate for the small area of a high-bandwidth PD and elevate the received signal-to-noise ratio (SNR) at a cost of narrowing down the receiver FOV. Angle diversity receiver (ADR), which is composed of multiple narrow-FOV detectors facing different directions, is one way to assure a wider FOV [10]. In [11], a wide-FOV receiver using fused fiber-optic tapers is introduced, which consists of hundreds of thousands of tapered optical fibers. An optical gain of 121.3 and overall FOV of 30° are reported.

An array of PDs accompanied with an optic is another favorable solution which can offer an improved SNR and a wider FOV compared to a single PD with a similar optic. Arrays can be either comprised of positive-intrinsic-negative (PIN) or avalanche photodiode (APD) detectors. They exhibit different performance in thermal noise limited or shot noise limited regimes [12]. The employment of them intensively depends on the applications. PIN arrays are more preferable for mobile scenarios because of their low biasing voltage [13]. The performance of an array also depends on the combiner technique, which can be equal gain combiner (EGC), selection combiner (SC), switched combiner (SWC) or the maximal ratio combiner (MRC). It is mathematically proven that even

This is a peer-reviewed, accepted author manuscript of the following article: Soltani, M. D., Kazemi, H., Sarbazi, E., Haas, H., & Safari, M. (2022). Optimal imaging receiver design for high-speed mobile optical wireless communications. In 2022 IEEE International Conference on Communications Workshops, ICC Workshops 2022 (pp. 439-444). IEEE. https://doi.org/10.1109/iccworkshops53468.2022.9814646

though an array of PDs augments more noise, employing more computationally complex algorithms such as MRC and SC can achieve a superior performance in comparison to a single-detector receiver [14], [15]. In [16], a receiver with 4×4 PD array is experimentally demonstrated data rate of 1 Gbps at a FOV of 10°. Umezawa *et al.* have reported an array of 8×8 PDs accompanied with a 15 mm diameter-lens, which manifests a FOV of 6° in [17]. They have achieved data rate of 25 Gbps at a distance of 10 m. These studies highlight the possibility of a high-speed mobile receiver by means of an array of PDs. However, the lack of a tractable analytical framework for designing of a high-speed receiver is deeply felt in the literature. In this paper, we initially derive a general model for SNR of a single array, where MRC technique is employed. Then, we extend the model for an array of arrays. Afterwards, we formulate an optimization problem to design an optimized receiver that can support a required FOV.

II. ADR-FOV Trade-off

The common architecture of a receiver for OWC includes three main elements: photodiode (PD), optics and transimpedance amplifier (TIA). The appropriate selection of these elements is crucial to address design requirements. For high-speed applications, high bandwidth PDs are more desirable, however, the higher the bandwidth, the smaller the sensitive area. This is known as the area-bandwidth trade-off and emphasizes that a high bandwidth PD may not collect sufficient power, especially when the beam spot area at the receiver is much larger than the PD area. Moreover, in a power-limited regime, high bandwidth PDs adds more noise to the system. This results in the SNR degradation. An optical element on top of the PD increases the collected power and enhances the SNR. However, the FOV of the receiver will be reduced due to the etendue law of conservation [9]. This principle introduces the gain-FOV trade-off. Finally a trade-off between the achievable data rate and receiver FOV is observed from the combining effects of the area-bandwidth and gain-FOV trade-offs, which will be discussed next.

A. Area-Bandwidth Trade-off

The bandwidth of PIN detectors can be obtained as [12]:

$$B = \frac{1}{\sqrt{\left(2\pi R_{\rm s}\epsilon_0\epsilon_{\rm r}\frac{A}{\ell}\right)^2 + \left(\frac{\ell}{0.44v_{\rm s}}\right)^2}}, \qquad (1)$$

where $\epsilon_0 = 8.85\times10^{-12}$ F.m^{-1} is the permittivity in vacuum, $\epsilon_{\rm r}$ is the relative permittivity of the semiconductor. The length of the depletion region and the PD area are denoted by ℓ and A, respectively. Also, the carrier saturation velocity is denoted by $v_{\rm s}$. The junction series resistance indicated by $R_{\rm s}$, varies from 7 Ω to 9 Ω depending on the PD size [18]. For the case that the PD is connected to a TIA with an input resistance of $R_{\rm L}$, then $R_{\rm s}$ in (1) should be replaced by the overall resistance $R_{\rm s} + R_{\rm L}$ [12].

The bandwidth equation given in (1) has an optimum depletion region length denoted as $\ell_{\rm opt}$ [12]. The bandwidth given in (1) at $\ell = \ell_{\rm opt}$ can be expressed as:

$$B = \frac{1}{C_{\rm t}d}, \qquad \text{where} \quad C_{\rm t} = \sqrt{\frac{4\pi R_{\rm s}\epsilon_0\epsilon_{\rm r}}{0.44v_{\rm s}}}. \qquad (2)$$

This equation provides an upper bound for bandwidth and other values of depletion region where $\ell \neq \ell_{\rm opt}$ result in a lower bandwidth.

B. Gain-FOV Trade-off

Optics elevate the collected optical power in cost of a narrower FOV. This principle is known as the gain-FOV trade-off. We employ an aspheric lens in this paper to develop an imaging receiver. Aspheric lenses are known to produce a precise and small beam spots. As an example, we consider the Thorlabs 354140-B aspheric lens. We calculate the beam spot radius after the lens and the FOV as functions of distance between the lens and the PD. These two functions are essential in the SNR analysis and optimum design of receiver. We note that the following analyses are extendable for any aspheric as well as thin lenses.

Let L denote the distance between the aspheric lens and the PD and $W_2(L)$ denote the beam spot radius after the lens. The beam spot radius can be well approximated by:

$$W_2(L) = b_1(f_{\rm b} - L) + b_0, \qquad (3)$$

where $f_{\rm b}$ is the back focal length of the aspheric lens, which is 820 μm for Thorlabs 354140-B. The two constants b_0 and b_1 depend on the diffraction limit and the clear aperture of the lens CA. We have obtained them using the OpticStudio [19] through measuring the beam spot radius at various L and then curve fitting, which are $b_0 = 1$ μm and $b_1 = 0.69$. It is required to evaluate the relation between FOV and L in reliable optical simulators. We use the OpticSudio for this purpose. For a required FOV, we obtain the proper L. The fitted curve to the results is:

$$L = a_3{\rm FOV}^3 + a_2{\rm FOV}^2 + a_1{\rm FOV} + a_0, \qquad (4)$$

where $(a_3, a_2, a_1, a_0) = (-0.08506, 6.142, -159.5, 1720)$ with a normalized root mean squared error of less than 10^{-4}.

III. SNR Analysis

To overcome the area-bandwidth trade-off, we consider small segmented high-speed PDs integrated together in the form of an array. We will then introduce an array of arrays as shown in Fig. 1 to ensure sufficient power is collected. Let the side length of each PD and the array be denoted by d and D, respectively. The fill factor (FF) of an array of $N_{\rm PD}$ PDs, which are arranged in a square lattice, can be obtained as:

$${\rm FF} = \frac{N_{\rm PD}d^2}{D^2}. \qquad (5)$$

We assume that the aspheric lens of radius $r_{\rm lns}$ is placed on top of the array. It is also assumed that each PD is followed by a high bandwidth TIA, since the output current of PIN

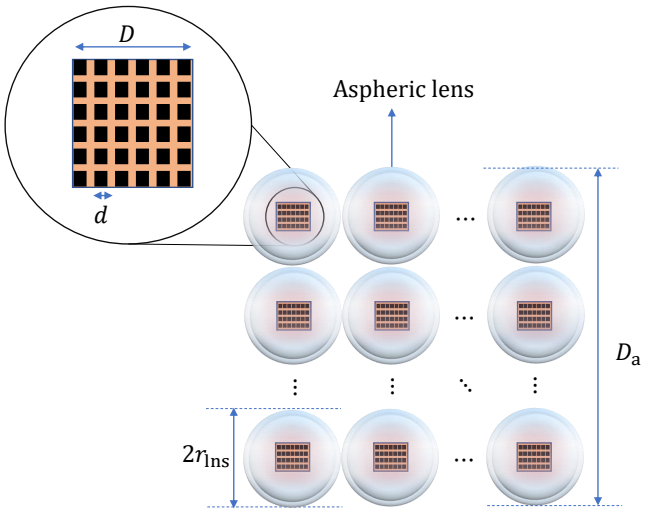

(a)

Fig. 1: Geometry of a $\sqrt{\mathcal{N}_a} \times \sqrt{\mathcal{N}_a}$ array of arrays.

detectors are typically so small. Under this assumption, the receiver bandwidth is limited by the PD's bandwidth.

Three types of noise can affect the performance of this receiver; thermal, shot and relative intensity noise [8], [20]. The dominant noise source is the TIA thermal noise whose variance is given by [10], [12]:

$$\sigma_n^2 = \frac{4k_b T F_n B}{R_f}, \tag{6}$$

where k_b is the Boltzmann constant, R_f is the feedback resistor of the TIA, T is temperature in Kelvin, F_n is the noise figure of the TIA and B is the bandwidth of the PIN detector.

Different combining methods such as maximum ratio combining (MRC), equal gain combining (EGC) and selection combiner (SC) can be used to integrate the output of PDs. Typically, MRC outperforms the other two techniques while requiring a more complex hardware circuit. In this study, we provide the analyses for MRC; however, they can be extended to EGC and SC in a similar way. In the following, we start by deriving the signal-to-noise ratio (SNR) of the MRC technique for a single array. We will then extend our analysis to a $\sqrt{\mathcal{N}_a} \times \sqrt{\mathcal{N}_a}$ array of arrays.

The SNR of MRC technique for a single array can be obtained as [21]:

$$\gamma_{MRC} = \sum_{i=1}^{N_{PD}} \gamma_i, \tag{7}$$

where γ_i is the SNR of the ith PD, which is:

$$\gamma_i = \frac{(R_{res} P_{r,i})^2}{\sigma_n^2}, \tag{8}$$

where R_{res} is the PD responsivity, σ_n^2 is the variance of noise given in (6), and $P_{r,i}$ denotes the received optical power of the ith PD. $P_{r,i}$ depends on the beam spot radius after the lens, $W_2(L)$, which is expressed by (3).

The radius of beam spot at the receiver plane is denoted by $W(z)$, where it is assumed that $W(z) \gg r_{lns}$. Thus, we can assume almost a uniform beam intensity over the whole area of the lens. Furthermore, ray-tracing simulations conducted in OpticStudio confirm that the beam after the lens has almost a uniform intensity profile. Accordingly, $P_{r,i}$ can be calculated as:

$$P_{r,i} = \iint_{\mathcal{A}_i} \frac{\xi P_{r,lns}}{\pi W_2^2(L)} \, dx \, dy, \tag{9}$$

where $\mathcal{A}_i$ is the area of beam that covers the ith PD. Also, $\xi = \xi_r \xi_p \xi_a$; with ξ_r representing the transmission coefficient of the lens; ξ_p depends on the definition of spot radius and $\xi_a = \mathrm{CA}^2/(2r_{lns})^2$. In (9), $P_{r,lns}$ is the power collected by the lens with the radius of r_{lns}. Based on the relation between $W_2(L)$, D and d, there are three separate cases for $P_{r,i}$, i.e.,

$$P_{r,i} = \begin{cases} \xi P_{r,lns} \rho, & W_2(L) \le \frac{1}{2} d, \\ \xi P_{r,lns} \dfrac{\mathcal{A}_i}{\pi W_2^2(L)}, & \frac{1}{2} d < W_2(L) \le \frac{1}{\sqrt{\pi}} D, \\ \xi P_{r,lns} \dfrac{d^2}{\pi W_2^2(L)}, & W_2(L) > \frac{1}{\sqrt{\pi}} D, \end{cases} \tag{10}$$

where $\rho = 1$ if N_{PD} is odd, and $\rho = 0$ otherwise. Substituting (10) into (8) and then into (7), the SNR of MRC technique for a single array is obtained as:

$$\gamma_{MRC} = \frac{1}{\dfrac{4k_b T F_n B}{R_f}} \left(R_{res} \xi P_{r,lns}\right)^2 \times \begin{cases} \rho, & W_2(L) \le \frac{1}{2} d, \\ \left(\dfrac{1}{\pi W_2^2(L)}\right)^2 \sum\limits_{i=1}^{N_{PD}} \mathcal{A}_i^2, & \frac{1}{2} d < W_2(L) \le \frac{1}{\sqrt{\pi}} D, \\ N_{PD} \left(\dfrac{d^2}{\pi W_2^2(L)}\right)^2, & W_2(L) > \frac{1}{\sqrt{\pi}} D. \end{cases} \tag{11}$$

Here, $\sum\limits_{i=1}^{N_{PD}} \mathcal{A}_i^2$ can be obtained numerically. However, it can be shown that:

$$\sum_{i=1}^{N_{PD}} \mathcal{A}_i^2 \approx \pi W_2^2(L) \mathrm{FF} d^2. \tag{12}$$

Therefore, (11) can be simplified as:

$$\gamma_{MRC} = \frac{1}{\dfrac{4k_b T F_n B}{R_f}} \left(R_{res} \xi P_{r,lns}\right)^2 \times \begin{cases} \rho, & W_2(L) \le \frac{1}{2} d, \\ \dfrac{d^2}{\pi W_2^2(L)} \mathrm{FF}, & \frac{1}{2} d < W_2(L) \le \frac{1}{\sqrt{\pi}} D, \\ N_{PD} \left(\dfrac{d^2}{\pi W_2^2(L)}\right)^2, & W_2(L) > \frac{1}{\sqrt{\pi}} D. \end{cases} \tag{13}$$

The SNR of EGC for a single array is given as:

$$\gamma_{EGC} = \frac{\left(\sum\limits_{i=1}^{N_{PD}} R_{res} P_{r,i}\right)^2}{N_{PD} \sigma_n^2}. \tag{14}$$

The SNR of MRC for an array of arrays of PIN detectors when thermal noise is the dominant noise part can be obtained by averaging over various tilts of receiver as follow:

$$\overline{\gamma}_{\mathrm{MRC}} = \frac{\sqrt{\mathcal{N}_{\mathrm{a}}}}{\frac{4k_{\mathrm{b}}TF_{\mathrm{n}}B}{R_{\mathrm{f}}}}(R_{\mathrm{res}}\xi P_{\mathrm{r,lns}})^2 \times \begin{cases} \mathrm{FF}, & W_2(L) \leq \frac{1}{2}d \\ \frac{d^2}{\pi W_2^2(L)}\mathrm{FF}, & \frac{1}{2}d < W_2(L) \leq \frac{1}{\sqrt{\pi}}D \\ N_{\mathrm{PD}}\left(\frac{d^2}{\pi W_2^2(L)}\right)^2, & W_2(L) > \frac{1}{\sqrt{\pi}}D \end{cases} \tag{15}$$

where $\mathcal{N}_{\mathrm{a}}$ is the total number of arrays of arrays, which are assumed to be arranged on a square lattice. It can be readily calculated as:

$$\mathcal{N}_{\mathrm{a}} = \left(\frac{D_{\mathrm{a}}}{2r_{\mathrm{lns}}}\right)^2, \tag{16}$$

where D_{a} is the side length of the array of arrays.

IV. Optimum Geometric Design of a High-Speed Receiver

In this section, we aim to determine the optimum side length of PDs in an array, i.e., d, as well as the distance between the lens and the array, L, which result in the maximum data rate. For this purpose, we have fixed the size of each single array to 400 μm $\times$ 400 μm (similar to [17]). Each single array is equipped with the aspheric lens 354140−B from Thorlabs[1]. The designed receiver should ensure the required FOV and BER. The optimum L can be specified according to the desired FOV. The optimum d is selected in such a way that it achieves the maximum data rate while fulfilling the required BER. We note that even though small PDs have higher bandwidth, they can add more noise to the system and degrade the SNR. On the other hand, large area PDs decreases the system bandwidth and consequently the achievable data rate. Such a behavior in a power-limited regime yields an optimum d that maximizes the data rate. Therefore, the optimization problem can be formulated as:

$$\max_{L,d} \quad R \tag{17a}$$

$$\text{s.t.} \quad \mathrm{FOV}(L) \geq \mathrm{FOV}_{\mathrm{req}}, \tag{17b}$$

$$\overline{\gamma}_{\mathrm{MRC}}(L,d) \geq \gamma_{\mathrm{req}}, \tag{17c}$$

$$d_{\min} \leq d \leq D\sqrt{\frac{\mathrm{FF}}{N_{\mathrm{PD}}}}, \tag{17d}$$

The first constraint leads to the condition that $L \leq L_{\max}$, where $L_{\max}$ can be obtained from (4). The second constraint enforces limitations on both the size of PDs and distance between lens and the array. In fact, SNR is directly proportional to d and L, where small values of d and L result in lower SNRs. Here, γ_{req} is the required SNR to ensure the BER is less than a target BER, i.e., $\mathrm{BER}_{\mathrm{req}}$. The size of each PD on the array is limited to $d_{\min}$ and $D\sqrt{\frac{\mathrm{FF}}{N_{\mathrm{PD}}}}$. The right side of the third constraint is obtained based on (5), which ensures the fill factor of the array is limited to FF. Note that the transmit power in this optimization problem is set to the maximum value that ensures the eye safety regulations, i.e., $P_{\mathrm{t}} = P_{\mathrm{t,max}}$ (for more information about $P_{\mathrm{t,max}}$ and eye safety considerations, we refer to [22]).

[1]This lens is just an example and other lenses can be also used.

TABLE I: Simulation Parameters.

Parameter	Symbol	Value
Load resistor	R_{L}	50 Ω
Feedback resistor	R_{f}	500 Ω
Junction series resistor	R_{s}	7 Ω [18]
Temperature	T	300° K
Carrier saturation velocity	v_{s}	4.8×10^4 m/s
TIA noise figure	F_{n}	5 dB
Transmission coefficient	ξ_{r}	0.88
Beam spot power ratio	ξ_{p}	0.5
Transmit power	P_{t}	10 mW
Side length of array	D	400 μm
Receiver responsivity	R_{res}	0.5

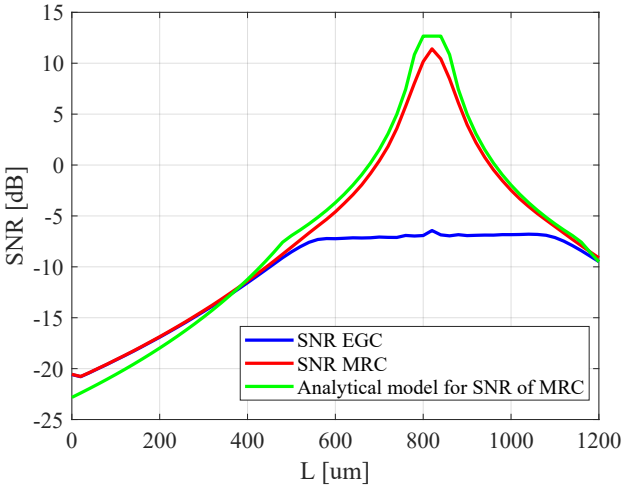

Fig. 2: SNR versus L for EGC, MRC and the analytical model based on (15) for $\mathcal{N}_{\mathrm{a}} = 64$.

V. Simulation Results

A single mode VCSEL transmitter is considered to operate at $\lambda = 850$ nm and with $w_0 = 5$ μm at 2 m from the receiver. The beam spot radius at the receiver side is 10 cm. The maximum size of receiver is set to be 2 cm. The fill factor of the array is chosen based on the designed array in [17], which is FF $= 0.64$. The lens parameters are adopted from the datasheet of the aspheric lens 354140−B [23]. We have also evaluated the transmission coefficient of the considered aspheric lens using OpticStudio software. The results show that the transmission coefficient is $\xi_{\mathrm{r}} = 0.88$. The rest of the simulation parameters are provided in Table I.

Fig. 2 show the SNR results of MRC and EGC obtained from OpticStudio simulator. The results are shown for $\mathcal{N}_{\mathrm{a}} = 64$ and $N_{\mathrm{PD}} = 64$. A remarkable gap of $\sim$ 18 dB can be observed between MRC and EGC techniques. This means that if we use the simple EGC technique instead of MRC, a greater number of array of arrays are required. Therefore, the size of

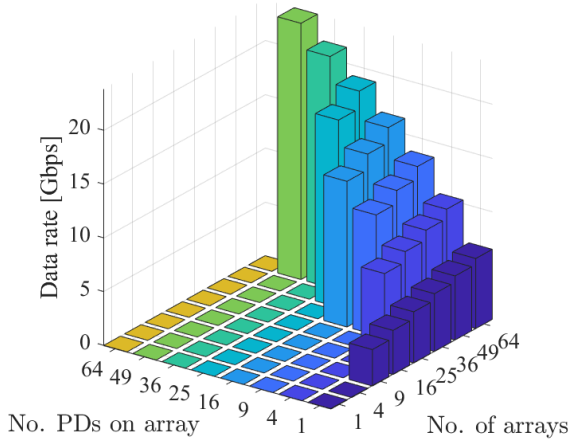

Fig. 3: Data rate versus Number of PDs and arrays using OOK modulation for the given FOV of 15°.

the receiver will be larger and it may not be applicable for mobile devices. A rough calculation shows that the size of a receiver with EGC should be 20 cm × 20 cm to achieve the same SNR as a receiver of size 2 cm × 2 cm using MRC when $L = 820$ μm. The analytical model for the SNR of MRC based on (15) are compared with the simulations in this figure, which proves the accuracy of our analytical model. One can simply rely on the proposed analytical model instead of those in OpticStudio ones and save plenty of time, particularly for applications such as machine learning.

Fig. 3 presents the achievable data rate versus the number of PDs in each single array and the number of arrays. The maximum data rate of 23.82 Gbps can be achieved for the given BER of 0.001 and the FOV of 15° using OOK modulation. It is assumed that the maximum length of receiver is 2 cm in these results. The single array that provides the maximum data rate includes 7×7 PDs with side length of 44.81 μm. This size of a PD provides a bandwidth of 11.91 GHz and it ensures the BER is less than 0.001. The achieved FF of the array is 0.61 which is very close to our target FF of 0.64. It can be observed that a minimum 3×3 array of arrays is required to ensure the required BER of 0.001 and the required FOV of 15° that achieves data rate of 3.38 Gbps.

The constraints given in (17) and the piecewise SNR function forms different areas. Fig. 4 illustrates these regions for $N_{\mathrm{PD}} = 49$, $\mathcal{N}_{\mathrm{a}} = 64$, $\mathrm{FF} = 0.64$, $\gamma \geq \gamma_{\mathrm{req}} = 9.55$ (this ensures $\mathrm{BER} \leq \mathrm{BER}_{\mathrm{req}} = 0.001$ for OOK modulation [10]) and $\mathrm{FOV} \geq \mathrm{FOV}_{\mathrm{req}} = 15°$ (or equivalently for $L \leq 820$ μm based on (4)). The cyan areas correspond to each sub-function of (15). The magenta areas are obtained based on the second constraint of (17) for each sub-function of SNR. These conditions guarantee the required SNR. The yellow areas indicate the third constraint in (17), which is 10 $\mu\mathrm{m} \leq d \leq 400\sqrt{\frac{0.64}{49}} = 45.7$ μm. The feasible region for the optimization problem can be found by looking into the intersection of these areas. The subsets in Fig. 4a and Fig. 4b depict the zoomed area of the intersection for convenience. The optimum values for d is the smallest in the intersection area to ensure the maximum data rate since $R = \frac{1}{C_{\mathrm{t}} d}$. Therefore, $d_{\mathrm{opt}} = 44.81$ μm and $L_{\mathrm{opt}} \in [785, 820]$ μm. We note that the choice of $L = 785$ μm yields the FOV of 16.2°.

Fig. 5 show the maximum data rate versus the required FOV. To have a fair comparison, the overall sensitive area of each configuration is almost equal so that the FF of 0.64 is achieved. Each subfigure represents a specific size of receiver (number of array of arrays). We note that neither of the 1×1 and 2×2 array of arrays are able to fulfill the BER and FOV requirement. Both 3×3 and 4×4 array of arrays can ensure the design requirements, only if each single array includes 1 PD. A 5×5 array of arrays with either 1×1 or 2×2 PD configurations is able to guarantee BER of less than 0.001 and required FOV of 15°. The rate-FOV trade-off can be observed in these results, where higher data rate are achievable in cost of lower FOV. For the 5×5 array of arrays, the 2×2 PD configuration is able to fulfill $\mathrm{FOV}_{\mathrm{req}} \leq 30°$ while the 1×1 PD configuration can support $\mathrm{FOV}_{\mathrm{req}} \leq 35°$. As shown in Fig. 5d, when the size of the receiver increases to an 8×8 array of arrays, each single array with 1 PD upto 7×7 PD arrangement are able to support the desired BER and FOV. The maximum data rate is related to an 8×8 array of arrays with 7×7 PDs on each single array, which is 23.82 Gbps. These maximum data rate can be achieved for $785 \leq L \leq 820$ μm. It worth mentioning that PD array of 8×8 is not able to satisfy the BER requirement. The reason is that the high bandwidth of the PDs adds more noise to the system. This is in accordance with the early statement that choosing high bandwidth PDs in a power-limited regime is not helpful as more noise will be added to the system. It is also noted that $\mathrm{FOV} \geq 30°$ can be achieved only with single-PD arrays at very close distances to the lens. Arrays with other PD configurations fail to assure $\mathrm{BER} \leq 0.001$. For a single PD equal to the size of the array (400×400 $\mu\mathrm{m}^2$), we can attain 70° FOV at $L \approx 0$ and a maximum data rate of 2.68 Gbps with an 8×8 array of arrays.

VI. Conclusions

In this study, we formulated an optimization problem to design a compact high-speed and wide FOV imaging receiver for OOK modulation. Furthermore, we derived analytically the optimum side length of PDs and the distance between an array and the lens. In order to have realistic simulations, we considered the practical aspects of receiver elements, such as the transmission coefficient of the lens. The simulations of the beam intensity profile and SNR are carried out using the OpticStudio software, which ensures the reliability of our results. We presented an analytical model for the SNR of MRC technique for array of arrays which was verified by the OpticStudio-based simulations. Insightful results and in-depth discussions are presented for OOK modulation. Simulation results confirm that with a square lattice arrangement of 8×8 array of arrays, we are able to achieve a maximum data rate of 23.82 Gbps data rate using OOK.

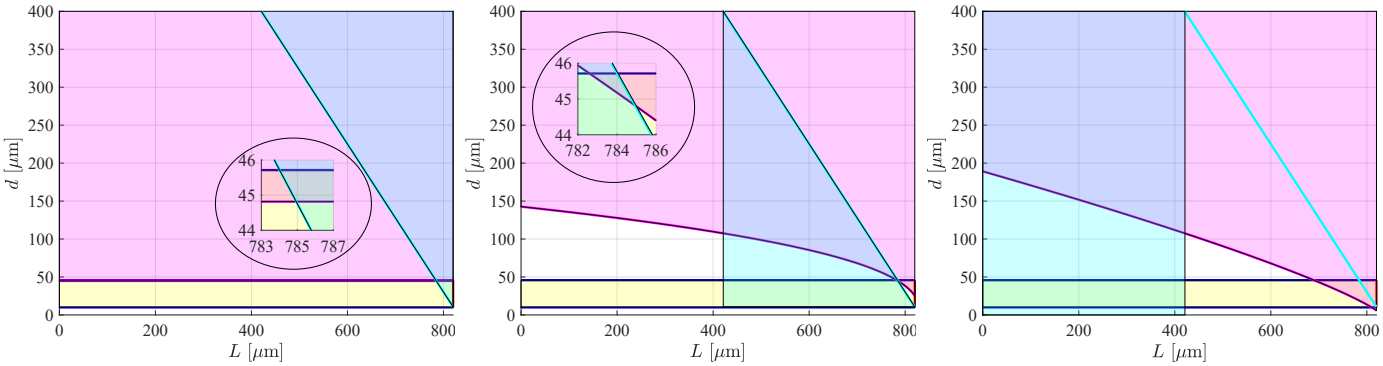

Fig. 4: Feasible region based on (a) first, (b) second and (c) third equations of SNR given in (15).

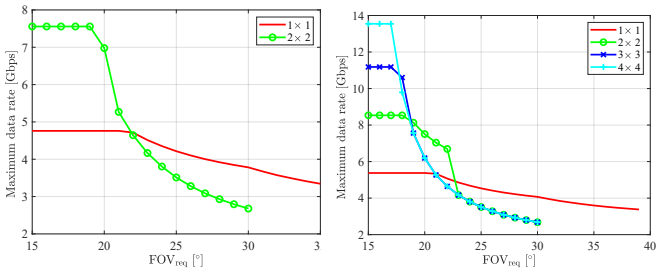

(a) Size of array of arrays: 5×5 (b) Size of array of arrays: 6×6

(c) Size of array of arrays: 7×7 (d) Size of array of arrays: 8×8

Fig. 5: Maximum data rate versus $\mathrm{FOV}_{\mathrm{req}}$ for different number of PDs on a single array and different sizes of array of arrays. OOK modulation and FF of 0.64 are assumed for these results.

ACKNOWLEDGMENT

The authors acknowledge financial support from Engineering and Physical Sciences Research Council (EPSRC) under grant EP/S016570/1 'Terabit Bidirectional Multi-User Optical Wireless System (TOWS) for 6G LiFi'.

REFERENCES

[1] Cisco white paper. (2020, Mar.) Annual Internet Report (2018–2023). [Online]. Available: https://www.cisco.com/c/en/us/solutions/collateral/executive-perspectives/annual-internet-report/white-paper-c11-741490.html

[2] "Cisco Annual Internet Report (2018–2023) White Paper," Cisco, Tech. Rep., Mar. 2020.

[3] X. Wu, M. D. Soltani, L. Zhou, M. Safari, and H. Haas, "Hybrid LiFi and WiFi Networks: A Survey," *IEEE Communications Surveys Tutorials*, vol. 23, no. 2, pp. 1398–1420, 2021.

[4] H. Haas *et al.*, "Optical wireless communication," *Philosophical Transactions of the Royal Society A: Mathematical, Physical and Engineering Sciences*, vol. 378, no. 2169, p. 20200051, 2020.

[5] Y. Hong *et al.*, "Demonstration of $>$ 1 Tbit/s WDM OWC with Wavelength-Transparent Beam Tracking-and-Steering Capability," *Opt. Express*, vol. 29, no. 21, pp. 33 694–33 702, Oct 2021.

[6] R. Singh *et al.*, "Design and Characterisation of Terabit/s Capable Compact Localisation and Beam-Steering Terminals for Fiber-Wireless-Fiber Links," *Journal of Lightwave Technology*, vol. 38, no. 24, pp. 6817–6826, 2020.

[7] T. Koonen *et al.*, "Ultra-High-Capacity Wireless Communication by Means of Steered Narrow Optical Beams," *Philosophical Transactions of the Royal Society A: Mathematical, Physical and Engineering Sciences*, vol. 378, no. 2169, p. 20190192, 2020.

[8] E. Sarbazi *et al.*, "A Tb/s Indoor Optical Wireless Access System Using VCSEL Arrays," in *Int. Symp. Pers., Indoor Mobile Radio Commun.*, 2020, pp. 1–6.

[9] J. Chaves, *Introduction to Nonimaging Optics*. CRC press, 2008.

[10] J. M. Kahn and J. R. Barry, "Wireless Infrared Communications," *Proceedings of the IEEE*, vol. 85, no. 2, pp. 265–298, 1997.

[11] O. Alkhazragi *et al.*, "Wide-Field-of-View Optical Detectors Using Fused Fiber-Optic Tapers," *Opt. Lett.*, vol. 46, no. 8, pp. 1916–1919, Apr 2021.

[12] S. B. Alexander, *Optical Communication Receiver Design*. Bellingham: SPIE Press, 1997.

[13] O. Kharraz and D. Forsyth, "Performance Comparisons Between PIN and APD Photodetectors for Use in Optical Communication Systems," *Optik*, vol. 124, no. 13, pp. 1493–1498, 2013.

[14] M. S. Bashir, "Free-Space Optical Communications With Detector Arrays: A Mathematical Analysis," *IEEE Transactions on Aerospace and Electronic Systems*, vol. 56, no. 2, pp. 1420–1429, 2020.

[15] M.-C. Tsai, M. S. Bashir, and M.-S. Alouini, "A Single Detector Versus an Array of Detectors Receiver in Free-Space Optical Communications: A Performance Comparison," 2021.

[16] T. Koonen *et al.*, "Novel Broadband OWC Receiver with Large Aperture and Wide Field-of-View," in *2020 European Conference on Optical Communications (ECOC)*, 2020, pp. 1–4.

[17] T. Umezawa *et al.*, "Large Submillimeter High-Speed Photodetector for Large Aperture FSO Receiver," *IEEE Journal of Selected Topics in Quantum Electronics*, vol. 28, no. 2, pp. 1–9, 2022.

[18] N. Dupuis *et al.*, "Exploring the limits of high-speed receivers for multimode vcsel-based optical links," in *OFC 2014*, 2014, pp. 1–3.

[19] Zemax, "Opticstudio." [Online]. Available: https://www.zemax.com/products/opticstudio

[20] H. Kazemi *et al.*, "A Tb/s Indoor Optical Wireless Backhaul System Using VCSEL Arrays," in *Int. Symp. Pers., Indoor Mobile Radio Commun.*, 2020, pp. 1–6.

[21] A. Goldsmith, *Wireless communications*. Cambridge university press, 2005.

[22] M. D. Soltani *et al.*, "Safety analysis for laser-based optical wireless communications: A tutorial," *arXiv preprint arXiv:2102.08707*, 2021.

[23] "Unmounted Aspheric Lens:354140-B," Thorlabs. [Online]. Available: https://www.thorlabs.com/newgrouppage9.cfm?objectgroup$_i d = 3811$